A NEW MITIGATION SCHEME TO RESIST PROGRESSIVE COLLAPSE OF RC STRUCTURES

Kamal Alogla[1], Laurence Weekes[1], Levingshan Augusthus-Nelson[1]

[1]School of Computer Science and Engineering, University of Salford, Manchester, United Kingdom

ABSTRACT

Reinforced concrete structures may be vulnerable to progressive collapse due to lack of sufficient continuous reinforcement. In most guidelines, general structural integrity requirements to reduce progressive collapse have been introduced, but the design of structures against progressive collapse has not been a major consideration. A mitigation scheme is proposed to increase resistance against progressive collapse. This involves the provision of additional reinforcement bars in the mid-layer of reinforced concrete beams. In the research reported here, four specimens were designed and tested subject to quasi-static loading conditions for a column removal scenario. One test specimen was made with conventional steel reinforcement and three specimens were made with additional steel reinforcement at the mid depth of the beam. The quasi-static behaviour of the test specimens were converted to a dynamic representation using an energy balance approach to obtain the progressive collapse load. Test results show that the proposed scheme significantly improves the ductility and collapse load of concrete beams subject to a column removal scenario.

INTRODUCTION

Progressive collapse is a situation where local failure is followed by collapse of adjoining members, which in turn causes global collapse and can eventually result in great loss of life and injury. Design of structures against progressive collapse has not been an integral part of structural design[1]. However, General Service Administration [2] and Unified Facilities Criteria Department of Defence [3] have suggested detailed requirements to reduce the likelihood of progressive collapse by altering the load path. Structural resistance against progressive collapse can be improved by increasing redundancy and continuity of the structure, and ductility of structural members. Redundancy will allow the structure to redistribute the load from the lost structural member to an alternative load path through the remaining structural members. This can only be achieved through continuity of the structure and the provision of adequate ductility. To achieve continuity in structural components, tie forces are required to tie the elements together so that they act as one unit. In general code provisions, structural integrity reinforcement is detailed to improve redundancy and ductility in structures[4].

When one of the critical load bearing elements is damaged or removed, connecting spans deflect until the rotational capacity provided by the adjacent beams or slabs is exhausted. Then, catenary action may allow the beam to carry vertical loads at large displacements. Catenary action is considered as the last line of defence for a structure to mitigate progressive collapse when a load bearing element is removed or damaged. Regan [5] concluded that the successful development of catenary action requires that the members in question possess not only tensile strength but also ductility, which is largely determined by the detailing of longitudinal reinforcement. The beam above a removed column undergoes three structural mechanisms: flexural action (FA), compressive arch action (CAA) and catenary action. Initially, all beams mobilize flexural action, which they are designed for and they are able to sustain the design load. When a column is removed, the span of the beam increases and in most cases leads to large deflection occurring in the beam. Compressive arch action, which enhances the flexural strength at critical sections, can be mobilized in the presence of axial compression provided by stiff lateral restraints[5]. At large deflections, catenary action can be mobilized. Orton [6] found that catenary action will not begin until the beam has reached a deflection approximately equal to the depth of the beam.

Existing buildings designed using design codes are prone to progressive collapse due to insufficient robustness in concrete frames. Consequently, numerous researchers such as Choi and Kim[7], Sadek et al.[8], Sasani and Kropelnicki[9], Su et al.[10], Yi et al.[11], Yu and Tan

[12] [13], Ren et al. [14] and Alogla et al.[15] have studied the structural behaviour of RC sub-assemblages subjected to column removal scenarios. Progressive collapse was studied theoretically by Izzuddin et al.[16], Xu and Ellingwood [17] and Li et al.[18]. The theoretical investigations have resulted in simplified models to estimate the ultimate collapse load[16]. Furthermore, researchers have been developing new methods to enhance the progressive collapse resistance. For example, Izadi and Ranjbaran [19] and Hadi and Alrudaini [20] proposed a scheme to resist progressive collapse by transferring the loads after column failure by suspending vertical cables at the top to a steel hat braced frame. Orton [6] suggested increasing the continuity of a beam by using carbon fibre reinforced polymer (CFRP). Yu and Tan [21] suggested adding steel rebar layers at the mid-height of the beam section, using partial hinges and partially de-bonding bottom reinforcement in the joint region.

From experimental studies [8,9,10,11], it was noticed that the top and bottom steel reinforcements at beam ends and middle joint, are vulnerable for fracture in the event of progressive collapse. Therefore, presence of additional steel layer will enhance the structural integrity by absorbing the released energy due to the redistributed load. In addition, the additional steel bars can increase the tying capacity of RC beams and tensile capacity in catenary action when it is developed.

In this paper, an economical scheme is proposed to increase progressive collapse capacity by adding two steel bars to the beam section throughout the beam length. In order to optimise the best location for the added steel layer, these bars will be added at different elevations within the beam section. The proposed scheme is easy to implement and will stand as an integral part of the structure, which allows for other structural members to function without any restrictions. In order to validate the proposed scheme, an experimental study of structural response of four RC sub-assemblages under a column removal scenario (CRS) were conducted and are presented here.

EXPERIMENTAL PROGRAM

A series of experiments were carried out to investigate progressive collapse resistance mechanisms and their capacities for RC beam-column sub-assemblages under CRS. In addition, the program studies the effect of the proposed mitigation scheme on progressive collapse resistance at compressive arch action and catenary action. Figure 1 shows the effect of column removal on a typical building. As seen in Figure 1, the bending moment significantly increases (approximately 4 times) due to doubling the span. Furthermore, the moment over the missing column reverses direction, positive where the beam was designed for negative moment. All these changes may not be considered in conventional design.

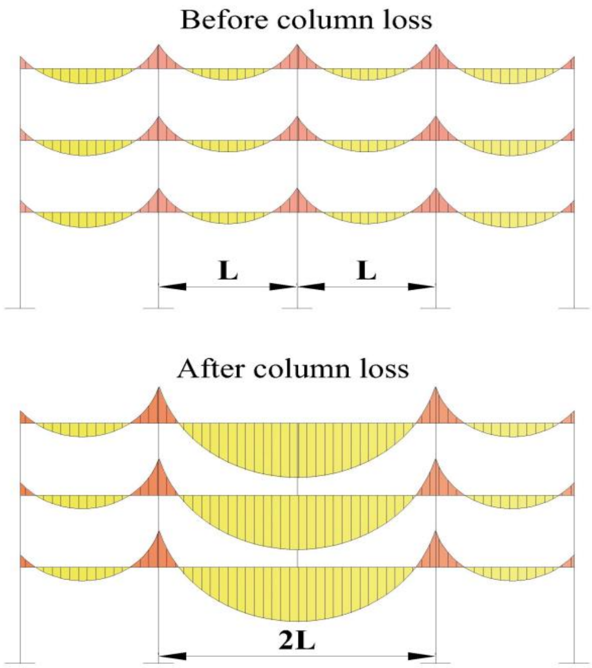

Figure 1: Moment distribution of a typical structure before and after column removal

DESIGN OF SPECIMENS

The specimens were designed to be extracted from the middle of a multi-storey, multi-bay frame building. Figure 2 shows part of a structure with the shaded area being directly affected by a removed column which represents the test specimen. A prototype frame building was designed and detailed according to ACI 318-05 [22] for non-seismic regions. The specimen was then scaled down to one-half of the prototype frame. In order to avoid the failure of the end support and focusing on structural mechanisms of the beam, the two end beam column stubs were enlarged to provide sufficient stiffness for the beam. Therefore, they had a much larger sectional size and provided an adequate space in which the longitudinal reinforcement could be well anchored. Figure 3 shows the dimensions and detailing of a typical specimen. The experimental program comprised the testing of four specimens: three specimens included the proposed new scheme and one specimen was constructed with conventional reinforcement detailing.

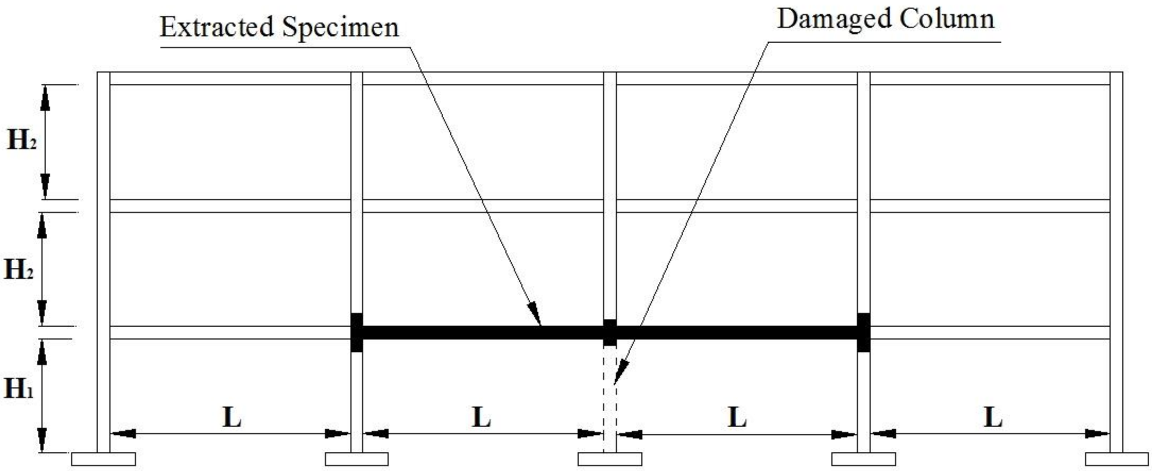

Figure 2: Test specimen in building front view

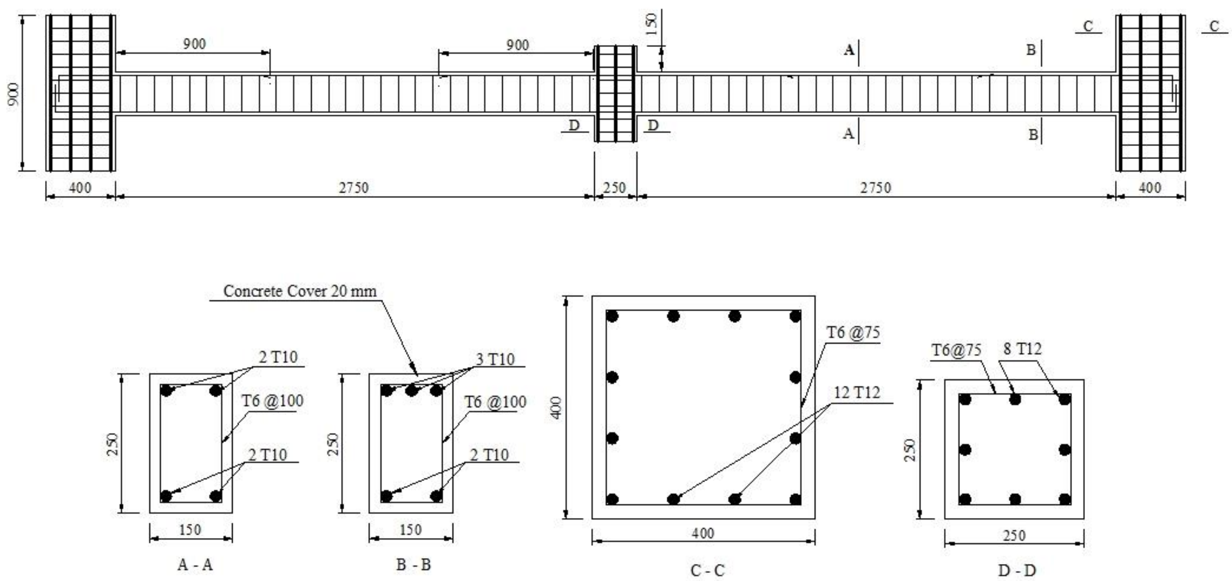

Figure 3: Conventional specimen dimensions and reinforcement details

PROPOSED SCHEME

Utilizing catenary action to provide a structure with greater load capacity than FA and CAA is one of the best options to mitigate progressive collapse of buildings. The catenary action mechanism requires that the concrete beam has significant continuity, ductility and sufficient tensile strength in the beam-column joint connection, which depends on the detailing of steel reinforcement. In order to provide a beam and joint with the required continuity, ductility and redundancy, the scheme proposes to add two additional longitudinal bars at different elevations of the beam section as shown in Figure 4. d and d' in figure 4 represent the effective beam depth and the distance from the extreme compression fibre of concrete to the centroid of compression reinforcement respectively.

For all specimens, the ratio of top steel reinforcement at the middle joint and at the beam ends was 0.72% using 3T10 steel bars, and the ratio of bottom steel reinforcement at the middle joint and at the beam ends was 0.48% using 2T10 steel bars. The additional steel bars are placed throughout the length of the specimen. The "T" symbol refers to deformed reinforcement bars, which have an area of 78.5 mm^2. Figure 4 shows each specimen's designation and details.

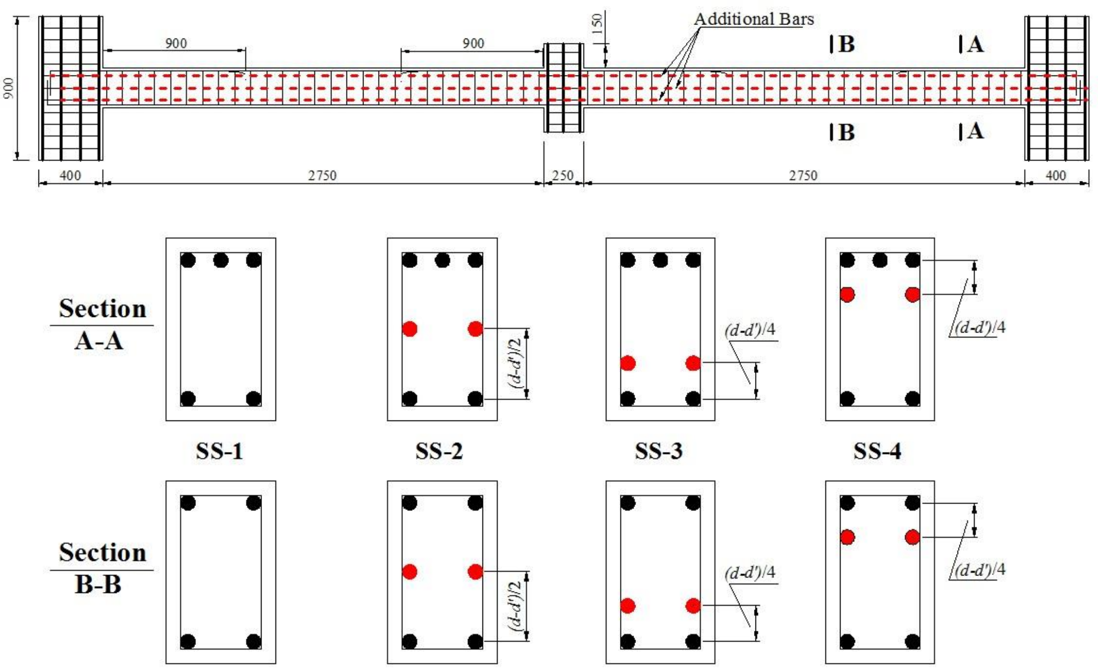

Figure 4: Designation and details of each specimen

TEST SETUP AND INSTRUMENTATION

Figure 5 shows a schematic plot for the loading test rig. To simulate the axial horizontal restraint for the beams, the ends of the specimens were connected to a steel frame by two load cells at each end, and these load cells were used to measure the horizontal forces that developed through the specimen during the test. In the vertical direction, a hinge roller support was used to restrain each end of the specimen. The hinge roller support reduces the effect of the vertical reaction on the horizontal reaction i.e. the vertical and horizontal reactions will be independent of each other.

The load cells used to measure the reactions in the horizontal direction had a capacity of 250kN in both tension and compression. The load was applied at the top of the middle joint using a hydraulic actuator with displacement control until total failure of the specimens. An actuator with a built-in load cell was attached into a steel frame fixed into the strong floor of the laboratory. A steel plate and roller was used to support the bottom of each of the end column stubs. Because of the slenderness of the specimens, a lateral steel restraint was provided near the centre of the specimens to prevent out-of-plane movement as shown in Figures 5 and 6. The testing frame was designed to provide adequate lateral stiffness to resist the expected compressive and tensile forces during CAA and catenary actions without frame failure. The stiffness of the lateral supports was at the level of $10^5\ kN/m$,which evaluated based on the test rig design.

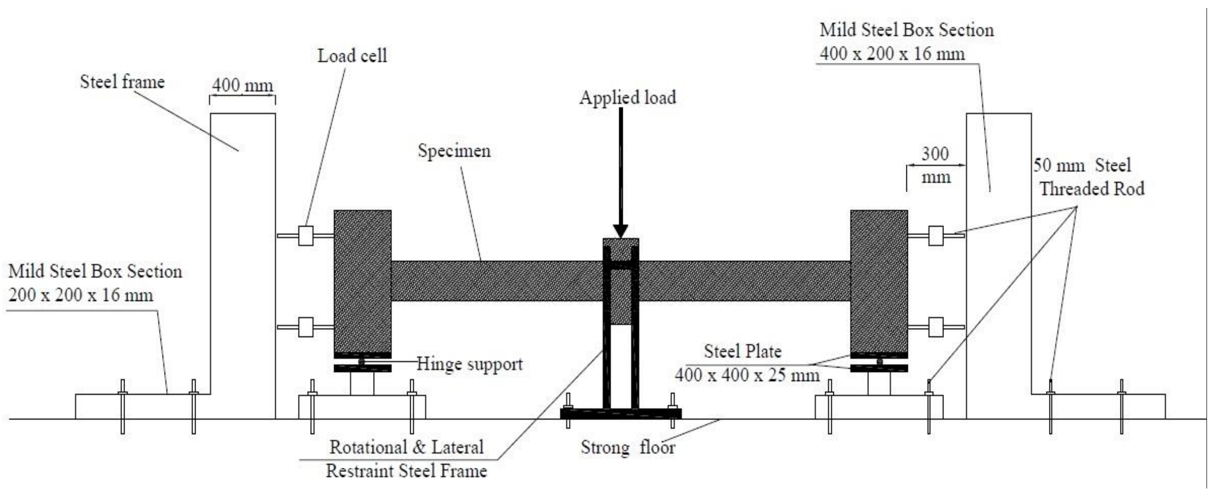

Figure 5: Schematic view of the test specimen and test rig

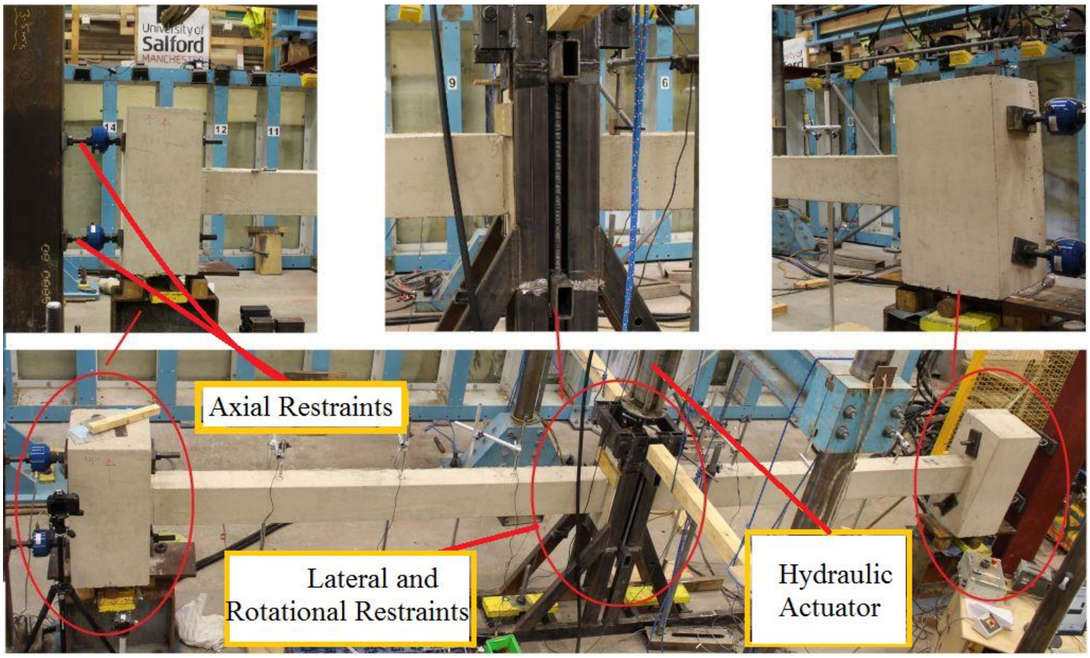

Figure 6: Test rig restraints

The RC sub-assemblage specimens were mounted with measuring instruments both internally and externally. The load imposed by the actuator was measured using an in-built load cell, which was connected in series with the hydraulic actuator jack. Seven external linear variable differential transformers (LVDT) were arranged to measure vertical displacement along the length of the specimens. Four load cells were attached to the column stubs at the ends of specimen to measure axial forces developed during the tests. These load cells have the ability to measure tension and compression forces. Figure 7 shows the lay-out of instrumentation along half of the sub-assemblage.

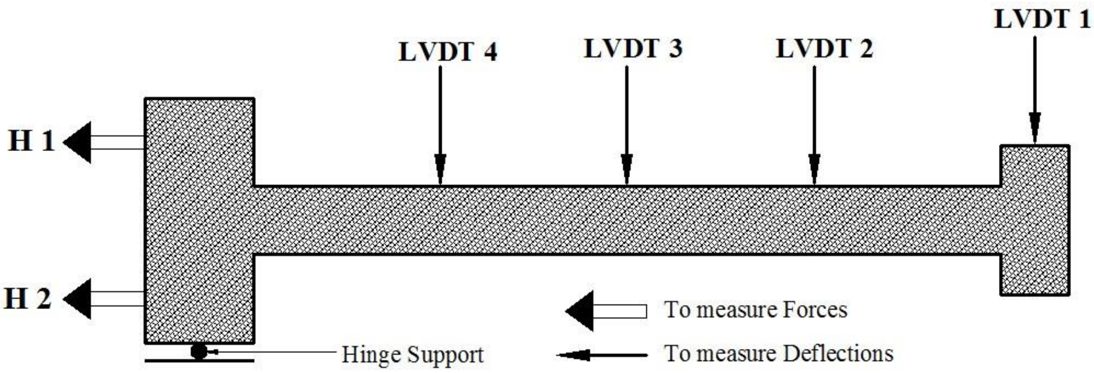

Figure 7: Arrangement of instrumentation

In order to monitor the development of internal stresses and forces for different structural mechanism phases, strain gauges were installed on the longitudinal steel reinforcement and attached at critical sections. These sections include faces of joints and additional steel reinforcement. Figure 8 shows the layout of strain gauges and their locations in the sub-assemblage specimens.

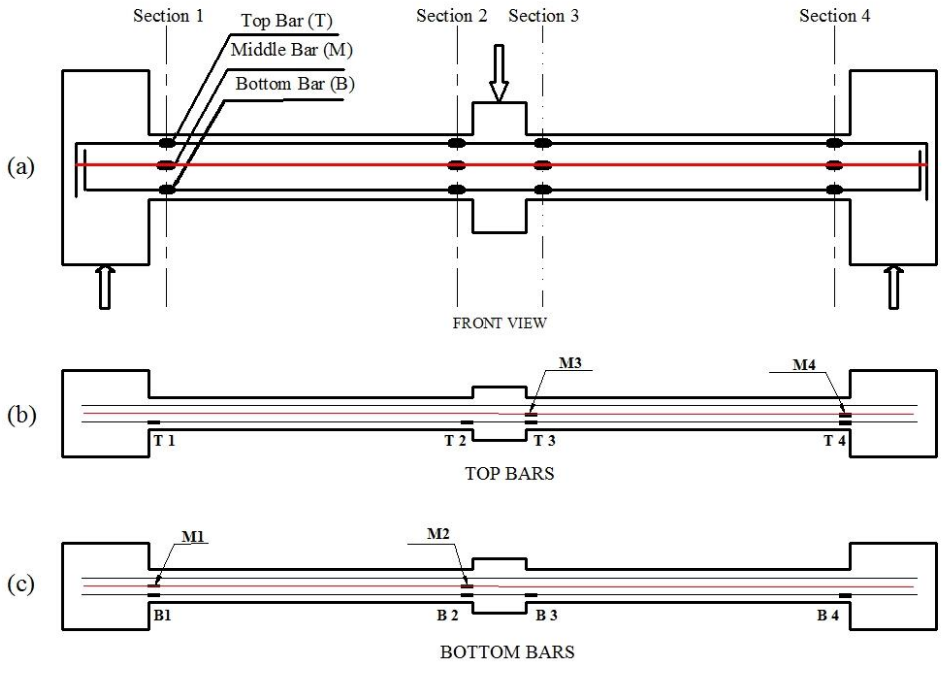

Figure 8: Locations of strain gauges. a) Front view, b) Top bars, c) Bottom bars

TEST PROCEDURE

The load was applied using a hydraulic actuator jack with a monotonic loading regime until total failure of the specimens. During the test, all reaction forces at each side (indicated as H1 and H2 in Figure 7) were measured using load cells, and the applied load was measured using the in-built load cell of the actuator. The displacement of the middle joint (MJD) and along the length of the beam was measured using LVDT's as shown in Figure 7. Therefore, the beam deflection at each load step could be determined, and axial forces developed through the beam could be calculated for each deflection value corresponding to each load step. In addition, strain gauges attached to the steel reinforcement were used to measure the strain in the steel bar at each load step. These strains can be converted into stresses and then to forces, which indicate the development of each resisting mechanism such as compressive arch action and catenary action.

The test data and results were collected and recorded simultaneously at a sampling rate of 1.0 Hz using an MTS data acquisition system. Relationships of MJD, horizontal reactions (axial forces) and bar strains are plotted for each magnitude of applied load for all specimens.

MATERIAL PROPERTIES

The construction of the specimens was divided into two batches. Two specimens were cast in each batch. For each specimen, three concrete cubes of dimension 100 x 100 x 100 mm were sampled, during the process of casting, to obtain concrete compressive strength. One cylinder of dimensions 300 mm height and 150 mm diameter was sampled and tested to obtain the modulus of elasticity. Also one prism of dimension 400 x100 x 100 mm was sampled to obtain the modulus of rupture. The compressive strength tests were carried out in accordance with BS1881-116, 1983[23]. The modulus of elasticity testing carried out in accordance with ASTM, C469-02[24].

According to the specimen design, the targeted concrete compressive strength at 28 days was 28 MPa, the average value of tested cubes was taken as listed in Table 1. For steel reinforcing bars, three samples of longitudinal bars were tested in tension. Steel reinforcement properties are listed in Table 2.

Table 1: Concrete mechanical properties

Specimens	Compressive Strength MPa	Modulus of Elasticity MPa	Modulus of Rapture MPa
SS-1 SS-2	26.8	23120	2.9
SS-3 SS-4	27.5	24205	3.0

Table 2: Steel properties

Steel Type	Yield Strength MPa f_y	Yield Strain	Elastic Modulus MPa Es	Ultimate Strength MPa f_u	Ultimate Strain	Hardening Modulus MPa E_h
T10	510	0.0026	196154	650	0.13	1099

TEST RESULTS AND DISCUSSION

In this section, experimental test results will be presented and illustrated at both global and local levels. Test results at the global level include the relationships between applied load and MJD, axial forces vs. MJD, failure mode and crack pattern. Axial forces were taken as the average of axial forces at both ends of the specimen. Test results at the local level include the relationship of rebar strains at critical sections with MJD. Moreover, test results have been differentiated and categorized according to the resistance mechanism for three stages: flexural, compressive arch action and catenary action.

For a building, “global” refers to the whole structure of the building system, while “local” refers to each structural member individually. For this section, “global” refers to the structural behaviour of the specimen, while “local” refers to the internal forces that developed during the test.

TEST RESULTS AT GLOBAL LEVEL

The overall structural behaviour of RC specimens is described by the relationships between the applied load against vertical deflection and the axial forces developed against vertical deflection. The deflected shape of the specimens can be illustrated by the deflection at specific points along the length of the beam at different stages of loading. Figure 9 shows the deflected shape curves of the specimens at specified load steps.

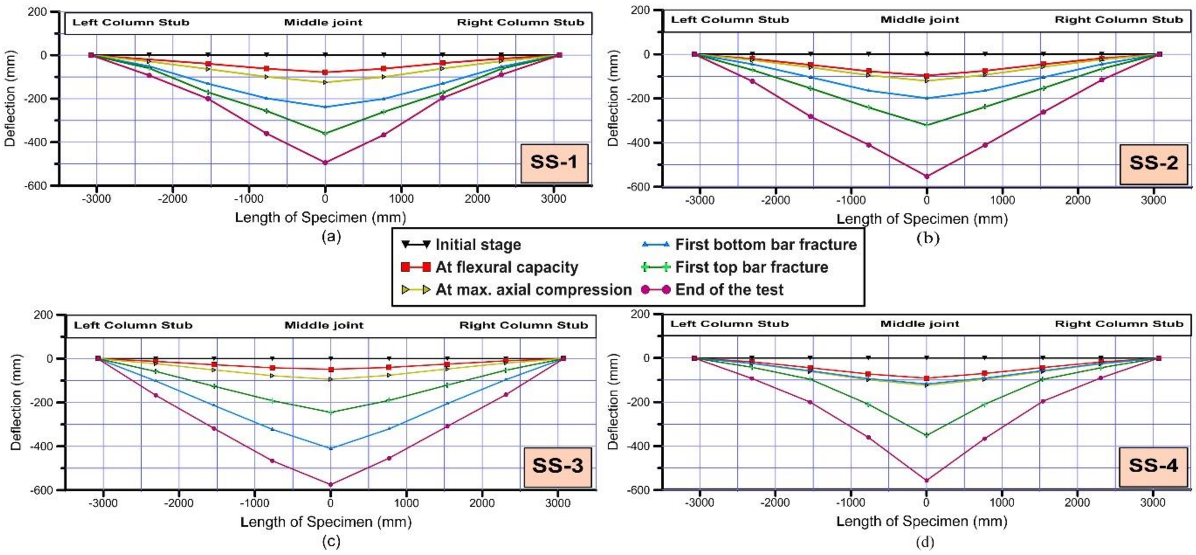

Figure 9: Beam deformation for (a) SS-1, (b) SS-2, (c) SS-3 and (d) SS-4

It can be seen from Figure 9 that all beams deflected symmetrically at both sides of the specimens. Also it can be observed that there is a large difference in displacement between the stage of bottom bar fracture and top bar fracture. This can be related to the formation of plastic hinges at the middle joint, which caused a large deflection at that stage. In contrast to other specimens, specimen SS-3 shows no sign of bottom bar fracture during flexural and compressive arch action. This can be explained by the presence of the additional steel reinforcement bars, which enhanced the force carrying capacity in the tension zone in the beam section, and resulted in fracture of the top bars firstly at a relatively large MJD. Deflection curves of specimen SS-4 showed a limited rotation at the beam ends, whilst being larger at the middle joint. This was due to the presence of additional steel bars at the top quarter of the beam section.

Based on the relationships of the applied load and the MJD of the specimens, the classification of three different mechanisms, flexural action, compressive arch action and catenary action, is shown in Figure 10. The overall trends of the load-displacement relationships for the specimens were quite similar despite having different steel detailing and minimal differences in concrete strengths, which results in different flexural capacity as can be seen from Figure 10. The peak flexural capacities were 34.0, 37.9, 37.2 and 36.7 kN for SS-1, SS-2, SS-3 and SS-4 respectively. After the peak loads were reached, plastic hinges were developed and bar fracture occurred. The abrupt large drops in the applied load shown in Figure 10 were due to subsequent fracture of steel reinforcing bars at either bottom or top of the beam section.

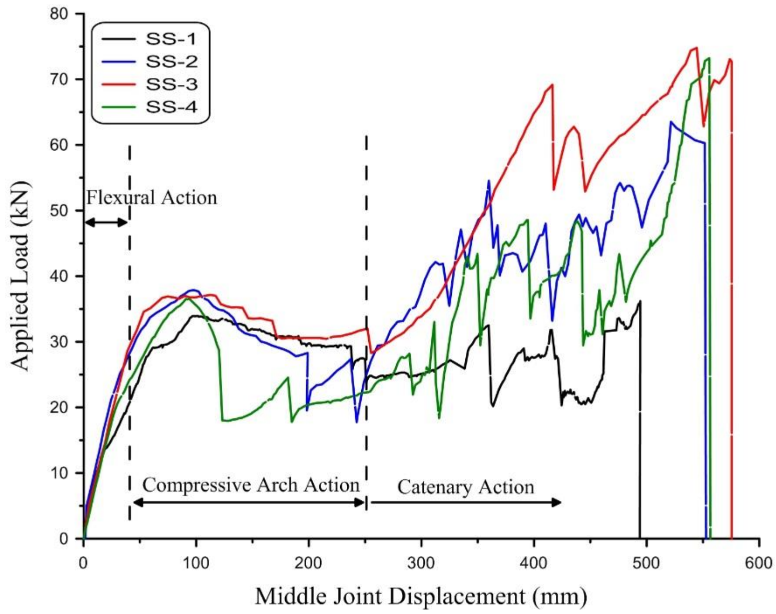

Figure 10: Applied load vs. MJD relationship of the specimens

Figure 10 shows the effect of the additional middle steel bars on the structural behaviour of RC specimens. Within compressive arch action, the applied load for all specimens was larger than specimen SS-1 by at least 8% for SS-4, and the peak applied load for specimen SS-2 was the largest. At the catenary action stage, the applied load for all specimens was larger than specimen SS-1 by at least 77% and the peak applied load for specimen SS-3 was the largest. This indicates that the effect of the middle layer on catenary action was greater than its effect on CAA. In other words, the additional middle layer is beneficial for an increase in tying capacity of the RC structures rather than flexural capacity. The final MJD for all specimens was larger than that for specimen SS-1 and the largest MJD was for specimen SS-3. This means that the additional steel bars can increase the rotational capacity for RC specimens and the optimum result can be obtained by placing the middle layer at a distance $(d - d')/4$ from the centre of the bottom bars.

Figure 11 shows the distribution of axial forces within the specimens. Within CAA, the axial forces developed were close to each other for all specimens. Transition points from CAA to catenary action ranged from 254 mm to 283 mm for SS-3 and SS-2 respectively. Due to the presence of additional longitudinal steel bars, the axial tension forces increased significantly. As listed in table 3, tensile force for specimen SS-3 was the largest, and it was more than twice the tensile force for specimen SS-1. Based on that and among the three locations of the additional steel bars, the highest tying capacity can be achieved in the event of progressive collapse by placing the middle layer at a distance $(d - d')/4$ vertically above the centre of the bottom bars.

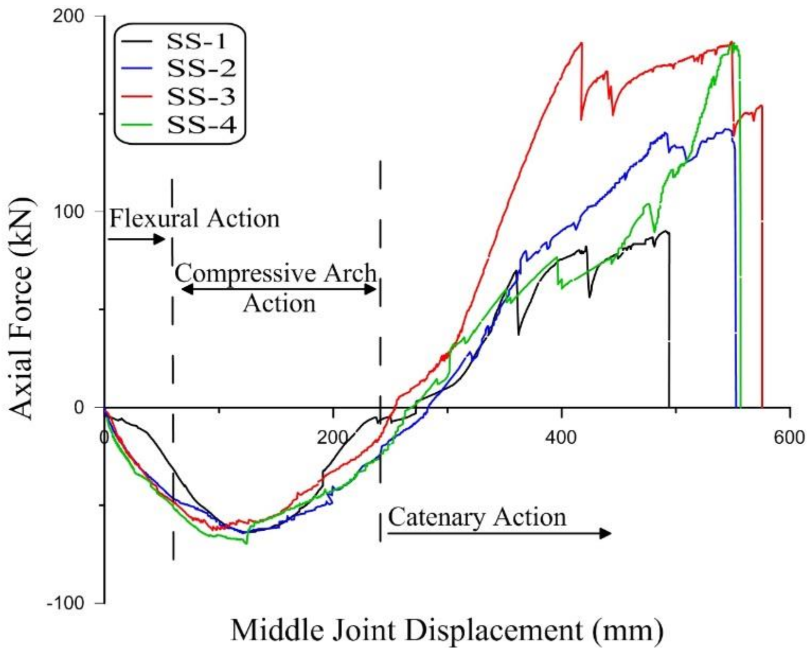

Figure 11: Axial force vs. MJD relationship of the specimens

Table 3: Forces with their MJD’s at critical stages

Specimen	Calculated flexural capacity with MJD		Max. load at CAA P_{com}			Max. Axial compression Force		Max. Axial Tension Force		Max. Load at Catenary Action		
	P_f (kN)	MJD (mm)	P_{com} (kN)	MJD (mm)	$\frac{MJD}{h}$	N_{com} (kN)	MJD (mm)	N_{ten} (kN)	MJD (mm)	P_{cat} (kN)	MJD (mm)	$\frac{MJD}{h}$
SS-1	28.0	57.9	34.0	101.0	0.40	63.8	125.6	89.2	494.0	36.2	494.0	1.98
SS-2	32.6	55.1	37.9	96.8	0.39	64.3	120.6	142.2	542.9	64.0	521.7	2.09
SS-3	32.2	48.2	37.2	86.8	0.35	62.7	94.6	186.9	549.0	75.6	549.0	2.20
SS-4	30.2	60.1	36.7	91.4	0.37	69.6	124.5	185.0	549.7	73.7	551.2	2.20

In table 3, the calculated flexural capacity was based on section analysis without considering the effect of axial forces.

Table 4 demonstrates a comparison with the specimen SS-1 to investigate the effect of these additional steel bars. It can be seen that with additional steel bars at the middle, the CAA capacity was 12% greater than for specimen SS-1. The largest increase at catenary action was 109% for specimen SS-3 compared to specimen SS-1. This indicates that the additional steel bars at the bottom quarter of the section can significantly increase progressive collapse capacity at catenary action.

In order to obtain progressive collapse capacity for each specimen, the non-linear static structural behaviour, which we will term 'quasi-static response', should be converted into non-linear dynamic behaviour. The proposed approach by Izzuddin et al. 2008 [16] was used to obtain progressive collapse capacity. This approach is based on energy equilibrium, which states that for the structure to be stable, the work done by applied gravity loads should be equal to the energy absorbed by the structure. In other words, the structure should have enough strain energy supply to absorb any energy demand caused by sudden loss of vertical support. In this approach, the effect of damping was neglected because the event of progressive collapse occurs in a very short time and the damping consumes little energy. Material strength enhancement due to strain rate, which is usually expressed in the form of a dynamic increase factor (DIF) is neglected in this approach. Yu et al. [25]concluded that the DIF is small and can be conservatively ignored for column removal scenarios. The converted non-linear dynamic behaviour is called the pseudo-static structural behaviour. Figure 12(a) shows both static and pseudo static responses for SS-1. For a given dynamic deflection u_d the applied dynamic load P_d can be obtained by equating the two hatched areas, which represent external work ($P_d \times u_d$) and strain energy ($\int_0^{u_d} P(u) d_u$). Pseudo-static structural behaviour can be obtained by repeating the process for each dynamic deflection. The accuracy of this approach has been validated by Tsai[26].

Table 4: Applied loads compared to specimen SS-1

Specimen	Applied Load (kN)			$\frac{P_{cat}}{P_{com}}$	$\frac{P_{com}}{P_{com(SS-1)}}$	$\frac{P_{cat}}{P_{cat(SS-1)}}$
	P_f	P_{com}	P_{cat}			
SS-1	28.0	34.0	36.2	1.065	1	1
SS-2	32.6	37.9	64.0	1.69	1.12	1.77
SS-3	32.2	37.2	75.6	2.03	1.10	2.09
SS-4	30.2	36.7	73.7	2.01	1.08	2.04

Figure 12(b) shows the pseudo-static structural behaviour of all specimens. The overall trends of the specimens were similar, but with different peak load values. With the exception of specimen SS-1, catenary action was able to increase the progressive collapse capacity. The largest enhancement was 67 % at catenary action stage for specimen SS-2.

Table 5 lists the peak loads with their corresponding deflections and the ratio of enhancement of catenary action stage. The lowest first peak was 25.9 kN for specimen SS-4 with lowest MJD of 120.7 mm.

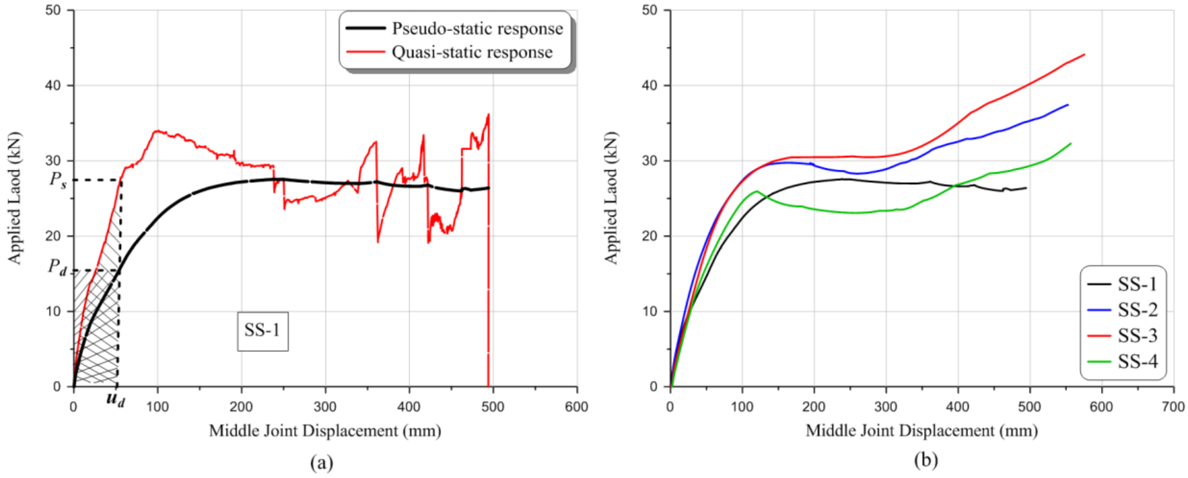

Figure 12: Pseudo-Static relationship for all specimens (a) Energy equilibrium approach for SS-1, and (b) Pseudo-Static curves for all specimens

It is clear that the new proposed scheme to resist progressive collapse was able to increase RC capacity at catenary action. The ultimate capacity can be achieved by adding steel bars to the bottom quarter of the beam section. The effect of adding steel bars at the top quarter of the beam section was marginal at the catenary action stage, while it decreases the capacity at CAA.

Table 5: Peak Loads with their corresponding deflections for all specimens

Specimen	First Peak Load at CAA		Max. Load At Catenary action		$\frac{P_{st}}{P_{st(SS-1)}}$	$\frac{P_{cat}}{P_{cat(SS-1)}}$
	P_{st} (kN)	MJD (mm)	P_{cat} (kN)	MJD (mm)		
SS-1	27.5	249.5	26.4	494.0	1	1
SS-2	29.7	163.8	37.4	553.0	1.08	1.42
SS-3	30.5	172.7	44.1	576.0	1.11	1.67
SS-4	25.9	120.7	32.3	557.0	0.94	1.22

CRACK PATTERN AND FAILURE MODE

The overall crack pattern and failure mode for the specimens were quite similar. At the flexural action stage, the cracks were concentrated at the beam-column joint interfaces, which are mainly caused by bending moments at these sections. Cracks developed during flexural action with the presence of compressive arch action beginning from the extreme tension face of the concrete, running vertically through the beam section and terminating at the location of the neutral axis. As the applied load increased, the neutral axis moved towards the compression face until the concrete crushed at the extreme surface in the compression zone. In contrast to flexural action, cracks during catenary action, started to develop throughout the beam length and passed completely through the beam section. With the increase of the applied load, wide cracks and bar fracture occurred at the beam-column joint interfaces.

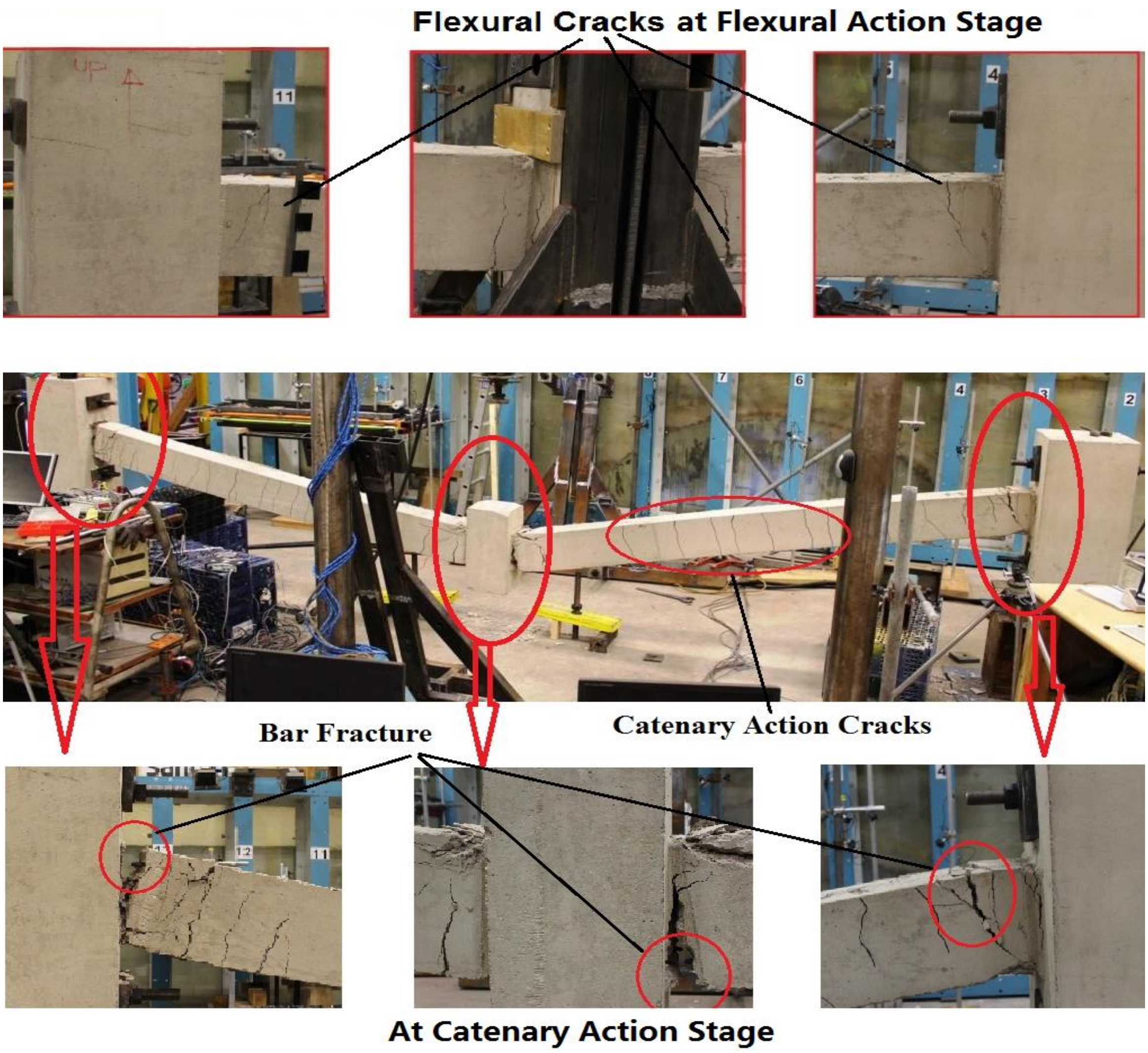

Figure 13: Crack pattern of specimen SS-1 at flexural and catenary action

It is worth mentioning that the cracks at catenary action were uniformly distributed along the beam length and that a large slip between the steel bars and concrete was observed at the beam-column joint interfaces. Figure 13 shows the crack pattern of specimen SS-1 at flexural action. It shows clearly the flexural cracks that developed at the beam-column joint interfaces. Figure 13 shows the crack pattern of specimen SS-1 at catenary action, which shows a uniform distribution of the cracks along the beam length.

Figure 14 shows crack development at different stages of loading for the left end of the specimen SS-3. Similar to the specimen SS-1, flexural cracks were developed at the beginning of the test followed by uniformly penetrating cracks along the length of the beam at catenary action stage. Flexural cracks were concentrated at the interfaces of beam-column joints. Flexural cracks developed from the extreme tension fibre of concrete, penetrated through the beam section and stopped at the location of neutral axis. Point “B” in Figure 14 represents the point of maximum axial compression force developed throughout the beam in which the indication of concrete crushing was clear. After that point, concrete spalling occurred indicated by the point “C”.

The failure of the specimen occurred after the point “F” at a deflection of 575.5 mm, indicated by a rapid increase in the deflection associated with a decrease in the applied load.

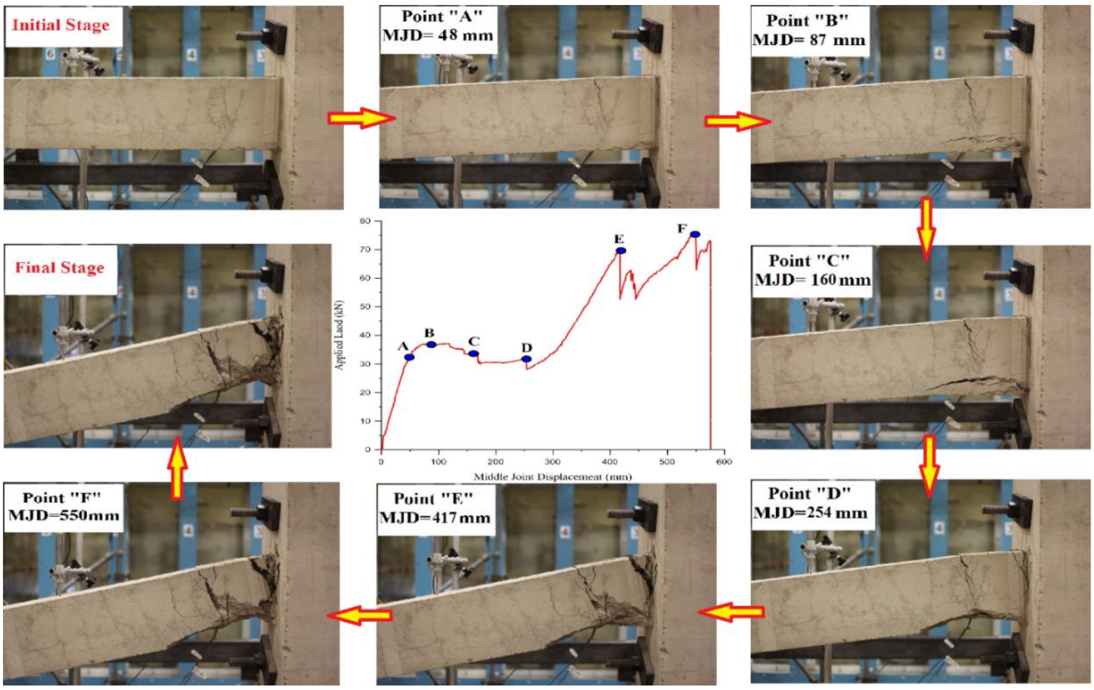

Figure 14: Crack development at the left beam end for specimen SS-3

TEST RESULTS AT LOCAL LEVEL

Bar strain measurements, which can be converted to bar forces, can shed light on the contributions of reinforcing bars to the mobilization of different mechanisms.

Development of stresses and forces at the additional steel bars provides insight as to how these bars affect the structural resistance mechanisms at both compressive arch and catenary action stages. Strain readings were converted into bar forces by multiplying the strains by the steel modulus of elasticity and the area of the bar. Converted bar forces were plotted against the MJD for each specimen.

Figure 15 shows the relationship between bar forces and MJD for specimen SS-1 and SS-3. The designations FT, FB and FM refer to the force of the top, bottom and middle bars respectively. For specimen SS-1, the transition in bar forces from compression to tension at sections 1 and 3 occurred at a deflection which was more than the deflection of the onset of catenary action for the specimen at global behaviour. The top bar force transition occurred with the fracture of the bottom bar and vice versa. It can be seen from Figure 15 (a-d) that the tensile forces during advanced catenary action were carried only by the bottom bars at the beam ends, and only by the top bars at the middle joint interfaces.

At the early stages of loading, the bottom bars yielded at sections 2 and 3, followed by fracture at both sections as shown in Figure 15. This means that the bottom bars are more vulnerable in the early stages of progressive collapse. At the mid stages of loading, it can be seen that the top bar is still carrying the loads at all sections, while at advanced stages of loading, both bars were fractured at two sections at least. It is clear that the need for additional bars at certain locations was crucial in order to reduce the probability of failure at critical sections.

For specimen SS-3, it can be seen from Figure 15 that the middle layer enhanced the tensile capacity of the beam by about 90.0 kN at catenary action, which is about 50% of the total force provided by the top and bottom steel bars. Due to the location of the added bars, they behaved similarly to the bottom bars, i.e. they carried compression forces at sections 1 and 4, while at sections 2 and 3 they carried tensile forces.

Figure 16 shows bar forces for each section at different stages of loading. These stages were chosen to represent each of the resisting mechanism phases. It should be mentioned that after fracture of some bars, residual strains remain, which are reflected as bar forces in the curves.

As shown in Figure 16b, for SS-1 at the catenary action stage, the bar at sections 2 and 3 was fractured and the values of the curve should be equal to zero.

It can be seen that both bars contribute to the tension forces developed at the catenary action stage. The change in the top and bottom bar forces during compressive arch action was smaller than the change in forces during catenary action, as can be seen from Figures 16a and 16b. The development of tension and compression forces for SS-1 and SS-3 at the top and bottom bars were nearly equal throughout the length of the beam, as can be seen from Figure 16c. From figure 16c, it is evident that the top and bottom bars at all sections were in tension, which indicates the action of the catenary stage.

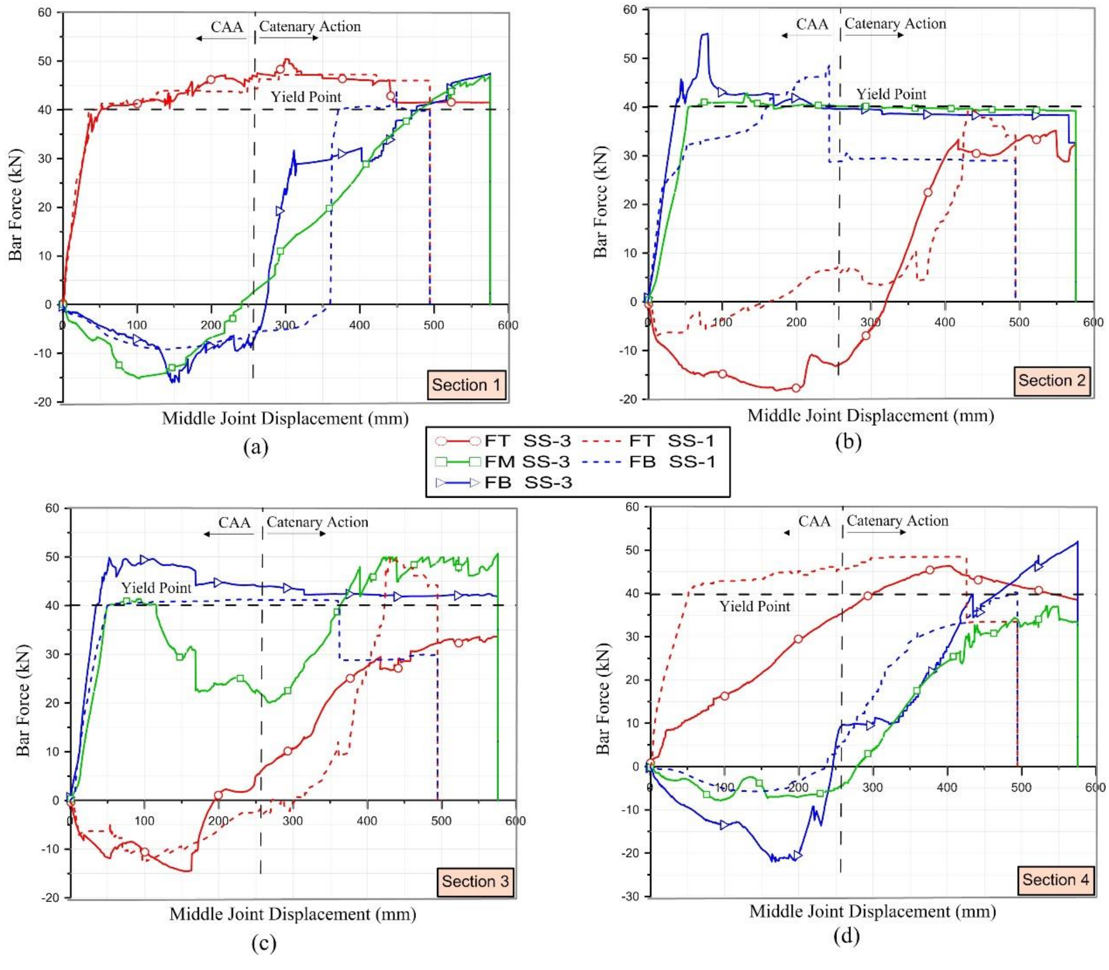

Figure 15: Bar Forces vs. MJD for specimen SS-1and SS-3

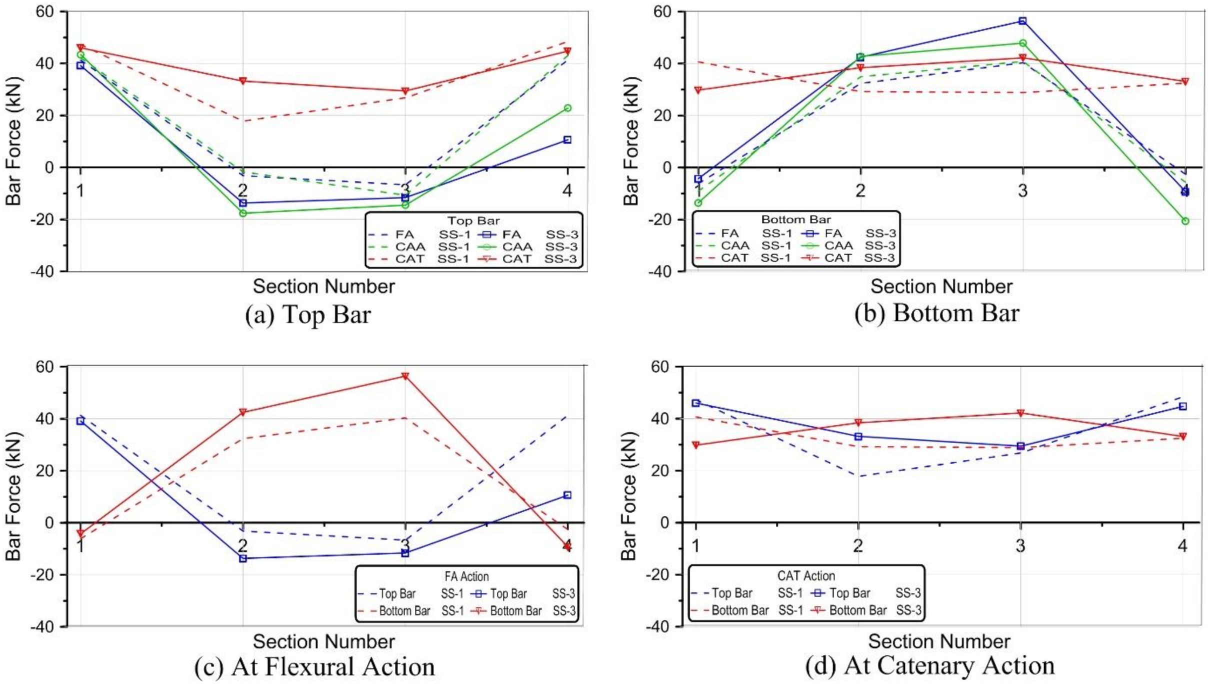

Figure 16: Bar forces for different resisting mechanisms for specimen SS-1 and SS-3

ANALYTICAL ULTIMATE LOAD CAPACITY AT CATENARY ACTION

Under concentrated applied load, it is expected that both bays of the sub-assemblage will remain straight until the total collapse, which is clearly shown in figure 8. Based on this expectation and figure 17, Li et al. [18]proposed a model to obtain ultimate load P_u at catenary action, which was then verified by Jian and Zheng [27], provided by equation 1

$$P_{u_{(Li)}} = \frac{(L_1 + L_2)v_u}{L_1 L_2} A_{th} f_u \qquad (1)$$

Where L_1 and L_2 are the spans of beam 1 and beam 2, respectively, v_u is the vertical displacement of the removed column, A_{th} is the area of the steel bars through the whole span, and f_u is the ultimate stress of the steel bars in the frame beams. Detailed determination of v_u can be found in Jian and Zheng[27].

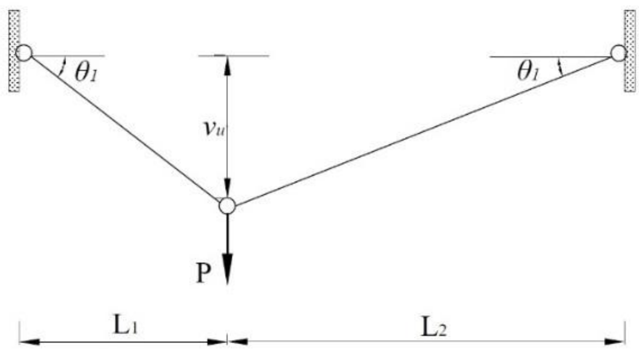

Figure 17 Schematic diagram for two bay beam at catenary action

PROPOSED LOAD CARRYING CAPACITY AT CATENARY ACTION

Based on experimental observation and results, top and bottom bar fractures have occurred. At large deflections, the tensile axial load was carried only by the bottom bars at the beam ends and the top bars at the middle joint as shown in figure 18(a). The ultimate load capacity at catenary action, P_u, can be obtained using a model, which is schematically shown in figure 18(b). The model is derived according to equilibrium at the middle joint considering fracture of steel bars shown in figure 18(a).

$$P = 2Nsin(\theta) \qquad (2)$$

$$\sin(\theta) = \frac{\delta_u}{L_2} \qquad (3)$$

$$N = f_u A_s \qquad (4)$$

The load P is assumed to be resisted only by the vertical component of the tensile force N, which is provided only by the intact steel bars. The tensile force contributions from the concrete, the top bars at the support and the bottom bars at the middle joint are neglected. Ultimate deflection, δ_u, can be calculated based on the total elongation of steel bars that can occur at the end of catenary action. Based on the assumption that the bar elongation is concentrated in the plastic hinge region, and the plastic hinge length model proposed by Mattock [28], the elongation, ΔL for each bay beam with two plastic hinges, can be obtained as follows (equation 5):

$$\Delta L = 2\varepsilon_{cu} l_p \quad (5)$$

Where ε_{cu} is the ultimate steel strain, l_p is the plastic hinge length. According to Mattock, $l_p = 0.5d + 0.05z$, where z is the distance from the point of maximum moment to the point of zero moment. From figure 18(b), δ_u can be obtained as follows:

$$\delta_u = \sqrt{L_2^2 - L^2} \quad (6)$$

$$L_2 = L_1 + \Delta L \quad (7)$$

$$L_1 = \sqrt{L^2 + (d - d')^2} \quad (8)$$

Where, L_2 is the final length of the bay beam at catenary action, L is the beam bay length, L_1 is the beam length at the fracture of the steel bars, d is the beam effective depth, and d' is the distance from the extreme compression fibre of concrete to the centroid of compression reinforcement.

Based on equation 8 for obtaining *L₁*, this model is only valid for a specimen designed using the conventional approach. This is because *L₁* is calculated on the beam section with the top and bottom steel bars only.

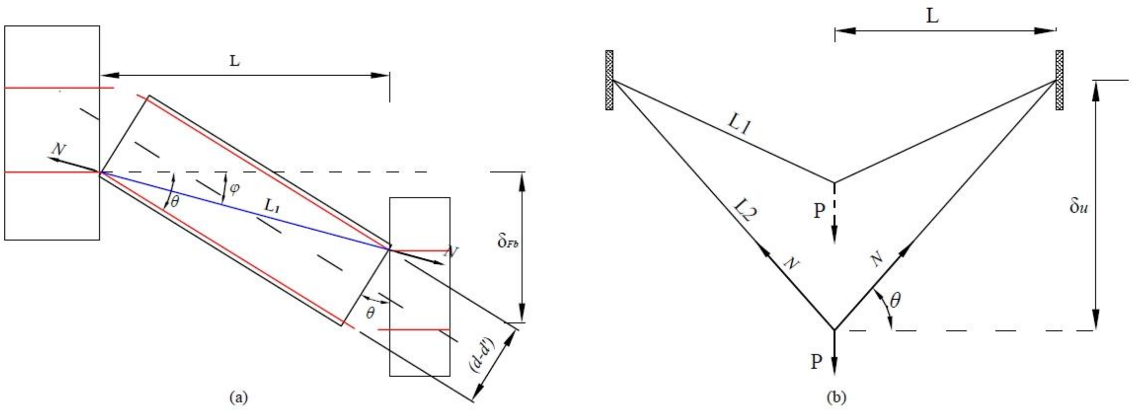

Figure 18: Schematic modelling of a specimen at Catenary Action

VALIDATION AND COMPARISON

Based on the geometry and material properties of specimen SS-1, the calculated values of vertical deflection v_u and δ_u were 494.5 mm and 494.2 mm respectively. Substituting these values in equations 1 and 2, $P_{u(Li)}$ and $P_{\boldsymbol{u}}$ were obtained and their values were 73.3 kN and 36.7 kN respectively. Compared to experimental values, it can be seen that the ultimate deflections were very close to the analytically calculated values. The calculated ultimate load from the proposed model is 1.4% greater than the experimental results, while it is 102% greater for $P_{u(Li)}$. Based on the analytical results, it can be concluded that the proposed model in this paper can accurately predict the ultimate deflection and applied load at catenary action. However, due to the complexity of progressive collapse phenomena, the imperfection of experimental data and some assumptions made in this paper, the proposed simplified model should be validated by more experimental or numerical data.

CONCLUSIONS

In this paper, four RC sub-assemblages were tested to investigate the progressive collapse resisting mechanisms of RC structures under a middle column removal scenario. On top of conventionally designed specimen SS-1, additional steel bars were added to the beam section at three different elevations aiming to improve the resistance capacity of RC frames against progressive collapse. The additional reinforcements were added at the mid-height of the beam section in SS-2. For specimen SS-3 and SS-4, the additional steel reinforcements were added at a distance equal to $(d - d^\wedge{}')/4$ from the centre of the bottom and top longitudinal reinforcement, respectively.

The experimental results showed that all specimens experienced three stages of resisting mechanisms: flexural, CAA and catenary action, and behaviour was dominated by flexure in the early stages of the response. With increased vertical displacement of the centre column, resistance was provided through the development of compressive diagonal axial forces or "arching action" due to the restraint on axial elongation of the beams by the end columns. With further increase in the vertical displacement, tensile axial forces developed in the beams, and the behaviour was dominated by catenary action.

Compared with the conventionally designed specimen, the capacity of specimens with modified detailing was 5% - 12% larger at CAA, while it was larger by about 52% - 109% at catenary action. The specimen with additional reinforcement in the middle, attained the largest ratio at CAA while the specimen with additional reinforcement at the bottom quarter attained the largest ratio at catenary action.

The bottom bars were more vulnerable to fracture in the early stages of progressive collapse due to the limitation in the rotational capacity of the beam section. . The additional bars near the bottom bars can reduce the probability of early bottom bar fracture. This is due to load sharing and increased tensile capacity, which in turn reduces the probability of progressive collapse.

The specimen with additional bars at the bottom quarter achieved larger deformation, and catenary action capacity in quasi-static response. The large deformation can be related to the increase in the rotational capacity of the beam column connection, which in turn increases the vertical projection of tensile forces at catenary action.

Pseudo-static results suggest that the presence of additional steel bars can increase progressive collapse capacity, and the maximum capacity can be attained when placing two additional steel bars at a distance of $(d - d')/4$ from the centre of the bottom reinforcement. The increase in progressive collapse capacity was 22% - 67%.

The overall crack pattern and failure mode for the specimens were quite similar. The failure of all specimens was characterized by (1) Crushing of concrete at compression zones during flexural action. (2) Development of flexural cracking during flexural and CAA. (3) Bar fracture at beam-column interfaces. (4) Large slippage between concrete and steel bars caused wide cracks at critical sections.

Based on experimental observation, a simplified model to predict ultimate deflection and applied load at catenary action was proposed. The proposed model, which accounts for bar fracture, can accurately predict load and deflection at catenary action.

ACKNOWLEDGMENTS

The authors gratefully acknowledge the funding by the Iraqi cultural attaché in London-UK.

REFERENCES

1. Kim, H., *Progressive collapse behavior of reinforced concrete structures with deficient details*. 2006: ProQuest.
2. GSA, *Progressive collapse analysis and design guidelines.* U.S. General Services Administration., 2003.
3. DOD, *Design of buildings to resist progressive collapse.* Unified Facilities Criteria (UFC)-Deaprtment of Defence, 2004.
4. Merola, R., *Ductility and robustness of concrete structures under accidental and malicious load cases*. 2009, The University of Birmingham.
5. Regan, P., *Catenary action in damage concrete structures.* ACI Special Publication, 1975. **48**: p. 191-224.
6. Orton, S., *Development of a CFRP system to provide continuity in existing reinforced concrete structures vulnerable to progressive collapse*. 2007: ProQuest.
7. Choi, H. and J. Kim, *Progressive collapse-resisting capacity of RC beam–column sub-assemblage.* magazine of concrete research, 2011. **63**(4): p. 297-310.
8. Sadek, F., et al., *Testing and analysis of steel and concrete beam-column assemblies under a column removal scenario.* Journal of Structural Engineering, 2011. **137**(9): p. 881-892.
9. Sasani, M. and J. Kropelnicki, *Progressive collapse analysis of an RC structure.* The Structural Design of Tall and Special Buildings, 2008. **17**(4): p. 757-771.
10. Su, Y., Y. Tian, and X. Song, *Progressive collapse resistance of axially-restrained frame beams.* ACI Structural Journal, 2009. **106**(5): p. 600-607.
11. Yi, W.J., et al., *Experimental study on progressive collapse-resistant behavior of reinforced concrete frame structures.* ACI Structural Journal, 2008. **105**(4): p. 433-439.
12. Yu, J. and K.H. Tan, *Progressive collapse resistance of RC beam-column sub-assemblages.* 2010.
13. Yu, J. and K.-H. Tan, *Experimental and numerical investigation on progressive collapse resistance of reinforced concrete beam column sub-assemblages.* Engineering Structures, 2013. **55**: p. 90-106.
14. Ren, P., et al., *Experimental investigation of progressive collapse resistance of one-way reinforced concrete beam–slab substructures under a middle-column-removal scenario.* Engineering Structures, 2016. **118**: p. 28-40.
15. Alogla, K., Weekes, L., and Augusthus-Nelson, L., *Progressive collapse resisting mechanisms of reinforced concrete structures.* Proceedings of the 5th International Conference on Integrity, Reliability and Failure. Porto, Portugal , 2016: p. 479-480.
16. Izzuddin, B., et al., *Progressive collapse of multi-storey buildings due to sudden column loss—Part I: Simplified assessment framework.* Engineering Structures, 2008. **30**(5): p. 1308-1318.

17. Xu, G. and B.R. Ellingwood, *An energy-based partial pushdown analysis procedure for assessment of disproportionate collapse potential.* Journal of Constructional Steel Research, 2011. **67**(3): p. 547-555.
18. Li, Y., et al., *An improved tie force method for progressive collapse resistance design of reinforced concrete frame structures.* Engineering Structures, 2011. **33**(10): p. 2931-2942.
19. Izadi, I.T. and A. Ranjbaran, *Investigation on a mitigation scheme to resist the progressive collapse of reinforced concrete buildings.* Frontiers of Structural and Civil Engineering, 2012. **6**(4): p. 421-430.
20. Hadi, M.N. and T.M.S. Alrudaini, *A new cable system to prevent progressive collapse of reinforced concrete buildings.* 2010.
21. Yu, J. and K.H. Tan, *Special detailing techniques to improve structural resistance against progressive collapse.* Journal of Structural Engineering, 2013. **140**(3): p. 04013077.
22. ACI-318. *Building code requirements for structural concrete (ACI 318-05) and commentary (ACI 318R-05).* 2005. American Concrete Institute.
23. BS1881-116, *Testing concrete. Method for determination of compressive strength of concrete cubes.* 1983.
24. ASTM-C469, *Standard Test Method for Static Modulus of Elasticity and Poisson's Ratio of Concrete in Compression.* ASTM International., 2002.
25. Yu, J., et al., *Dynamic Progressive Collapse of an RC Assemblage Induced by Contact Detonation.* Journal of Structural Engineering, 2014.
26. Tsai, M.-H., *An analytical methodology for the dynamic amplification factor in progressive collapse evaluation of building structures.* Mechanics Research Communications, 2010. **37**(1): p. 61-66.
27. Jian, H. and Y. Zheng, *Simplified models of progressive collapse response and progressive collapse-resisting capacity curve of RC beam-column substructures.* Journal of Performance of Constructed Facilities, 2014. **28**(4): p. 04014008.
28. Mattock, A.H., *Rotational capacity of hinging regions in reinforced concrete beams.* Special Publication, 1965. **12**: p. 143-181.